Dielectric relaxation and electronic structure of $Ca(Fe_{1/2}Sb_{1/2})O_3$

Alo Dutta and T. P. Sinha
Department of Physics, Bose Institute, 93/1 Acharya Prafulla Chandra Road, Kolkata 700009, India

Santiranjan Shannigrahi
Institute of Materials Research and Engineering (IMRE), 3 Research Link, Singapore 117602, Singapore
(Received 5 January 2007; revised manuscript received 28 June 2007; published 19 October 2007; publisher error corrected 22 October 2007)

The frequency-dependent dielectric relaxation of calcium-iron-antimonate $[Ca(Fe_{1/2}Sb_{1/2})O_3]$ (CFS) ceramic, synthesized by a solid-state reaction technique is investigated in the temperature range from 143 to 463 K by alternating-current impedance spectroscopy. The x-ray diffraction of the sample at room temperature shows a monoclinic phase. Using Cole-Cole model, an analysis of the imaginary part of the dielectric permittivity with frequency is performed assuming a distribution of relaxation times. The activation energy calculated from the frequency dependence of loss spectra is found to be $\simeq 0.60$ eV, which suggests that the bulk conduction in CFS is due to polaron hopping based on the electron carriers. The scaling behavior of the imaginary part of the electric modulus (M'') suggests that the relaxation describes the same mechanism at various temperatures. We studied the electronic structure of the CFS using x-ray photoemission spectroscopy (XPS). The XPS spectrum was analyzed by the first-principles full-potential linearized augmented plane wave method.

DOI: 10.1103/PhysRevB.76.155113 PACS number(s): 71.20.−b, 77.84.−s, 79.60.−i, 71.15.Mb

I. INTRODUCTION

Simple perovskite compounds have the chemical formula ABO_3. In the cubic phase, the oxygen atoms form a cubic lattice of corner-sharing octahedra with the B cations at their centers, while the A cations form a second interpenetrating cubic sublattice located at the 12-fold coordinated sites between octahedra. Interestingly, most of the perovskite compounds that are of greatest technological interests are not simple systems, but rather complex oxides with two different kinds of B atoms, such as $A(B'B'')O_3$.

The dielectric constant of a material (dielectric) changes due to the change of polarization by an applied electric field. In alternating-current impedance spectroscopy, this change in polarization is time dependent. Because of the resistance (resistivity) to the motion of atoms in the dielectric, there is always a delay between changes in field and changes in the polarization, which gives the dissipation factor $\tan\delta$ and is proportional to the energy absorbed per cycle by the dielectric from the field.

In numerous complex oxides with the perovskite structure, low-frequency dielectric relaxation behavior has been observed.[1–7] The low-temperature dielectric relaxation in these oxides is not related to a phase transition and probably related to a series of excitations in the solids.[8] Hence, the study of electronic structure (i.e., the spectral density function and the density of states) of such type of systems may be considered essential. In the present work, dielectric and photoelectron spectroscopy studies of calcium iron antimonate, $Ca(Fe_{1/2}Sb_{1/2})O_3$ (CFS), ceramic prepared by a solid-state reaction technique are presented. The information associated with the spectral density function is accomplished by x-ray photoemission spectroscopy (XPS), while the density of states (DOS) is obtained by first-principles calculation based on density functional theory (DFT) under generalized gradient approximation (GGA) employing full-potential linearized augmented plane wave (FLAPW) method. The experimental results are compared to the calculated electronic structure. We have attempted to clarify the electronic structure of the system as it emerges from a combined spectroscopic study and first-principles calculations.

II. EXPERIMENT

In analogy to our previous work,[5–7] the ceramic method was employed for the synthesis of CFS. The raw chemicals used in this study were reagent grade $CaCO_3$, Fe_2O_3, and Sb_2O_5. The mixed raw chemicals in the stoichiometric ratio were calcined in a Pt crucible at 1200 °C for 9 h and brought to room temperature under controlled cooling. The calcined sample was pelletized into a disk using polyvinyl alcohol as binder. Finally, the disks were sintered at 1250 °C for 4 h and cooled down to room temperature by adjusting the cooling rate.

The x-ray powder diffraction pattern of the sample taken at room temperature is shown in Fig. 1. All the reflection peaks of the x-ray profile were indexed and lattice parameters were determined using a least-squares method with the help of a standard computer program (POWD). A good agreement between the observed and calculated interplanar spacing (d values) suggests that the compound is having a monoclinic structure at room temperature with $\beta = 97.53°$ ($a = 5.9565$ Å, $b = 6.9847$ Å, and $c = 5.8047$ Å). X-ray diffraction confirms that the specimen is single phase. To measure the electrical properties, gold electrodes were formed on both surfaces of the sintered disk. The frequency dependence of the dielectric constant and loss tangent was obtained using an *LCR* meter in the temperature range from 143 to 463 K and in the frequency range of 50 Hz to 1 MHz.

The XPS experiments have been done using XPS (VG ESCALAB 2201-XL Imaging System, England). XPS pro-

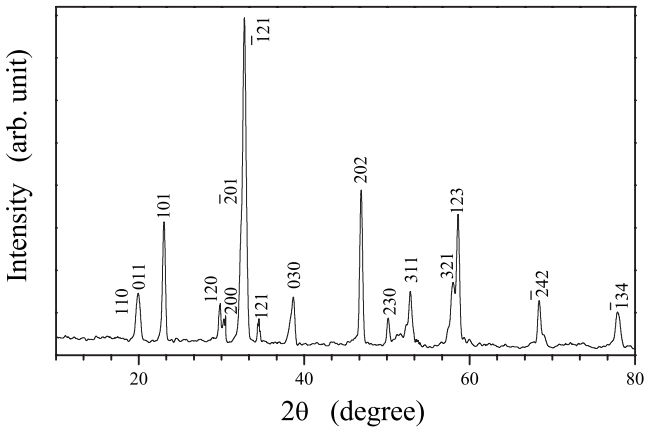

FIG. 1. X-ray diffraction pattern of $Ca(Fe_{1/2}Sb_{1/2})O_3$ at room temperature.

files of the samples were obtained using an Al K_α source (1486.6 eV). The C1s peak was used as the reference standard.

The electronic structure of CFS was calculated by using a density functional calculation within the generalized gradient approximation on the basis of the full-potential linearized augmented plane wave method.[9] The angular momentum projected local densities of states for CFS were obtained by using 28 k points inside the irreducible Brillouin zone for integration.

III. EXPERIMENTAL RESULTS AND DISCUSSION

The angular frequency $\omega(=2\pi\nu)$ dependence plots of the real (ϵ') part of the complex dielectric permittivity $(\epsilon^\star)$ and the dielectric loss tangent (tan δ) of CFS at several temperatures between 173 and 403 K are plotted in Fig. 2. A relaxation is observed in the entire temperature range as a gradual decrease in $\epsilon'(\omega)$ and as a broad peak in tan $\delta(\omega)$.

Relaxation phenomena in dielectric materials are associated with a frequency-dependent orientational polarization. At low frequency, the permanent dipoles align themselves along the field and contribute fully to the total polarization of the dielectric. At higher frequency, the variation in the field is too rapid for the dipoles to align themselves, so their contribution to the polarization and, hence, to the dielectric permittivity can become negligible. Therefore, the dielectric permittivity $\epsilon'(\omega)$ decreases with increasing frequency.

It is evident from Fig. 2(b) that the position of loss peak tan δ_{max} (centered at the dispersion region of ϵ') shifts to higher frequency with increasing temperature and that a strong dispersion of tan δ exists in CFS. The temperature dependence of the imaginary (ϵ'') part of the dielectric constant plotted in Fig. 3 implies that the hopping of charge carriers plays an important role in their transport processes because a loss peak is an essential feature of the charge carrier hopping transport.

It seems clear that the width of the loss peaks in Fig. 2(b) cannot be accounted for in terms of a monodispersive relaxation process but points toward the possibility of a distribu-

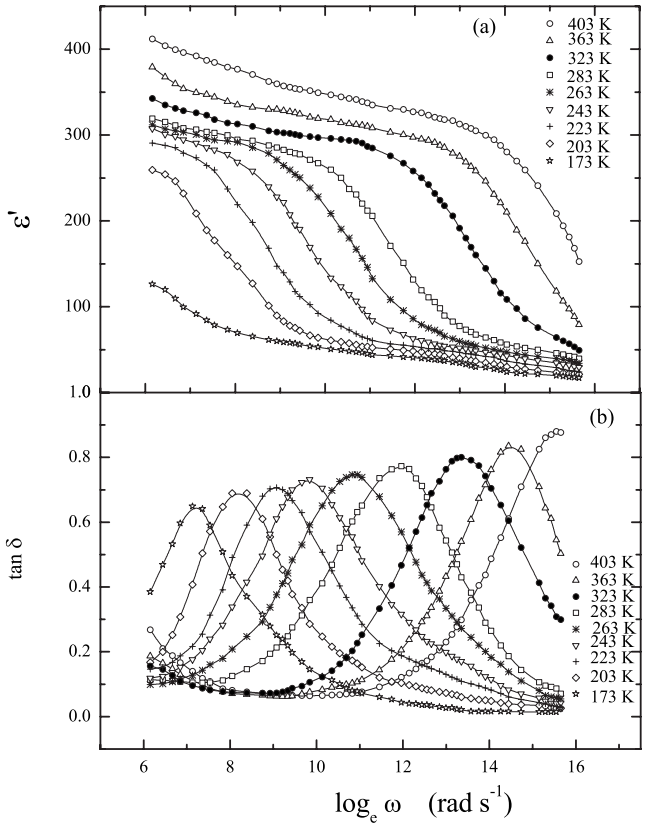

FIG. 2. Frequency dependence of the (a) ϵ' and (b) tan δ of $Ca(Fe_{1/2}Sb_{1/2})O_3$ at various temperatures.

tion of relaxation times. If $g(\tau,T)$ is the temperature dependent distribution function for relaxation time, the complex dielectric constant can be expressed as[10–13]

$$\epsilon^\star - \epsilon_\infty = \epsilon(0,T)\int_0^\infty g(\tau,T)\frac{d(\ln\tau)}{1-i\omega\tau}, \tag{1}$$

giving

$$\epsilon'' = \epsilon(0,T)\int_0^\infty g(\tau,T)\frac{d(\omega\tau)}{1+\omega^2\tau^2}, \tag{2}$$

where $\epsilon(0,T)$ is the low-frequency dielectric constant. Thus, the spectrum of dielectric loss gives direct information about $g(\tau,T)$.

One of the most convenient ways of checking the polydispersive nature of dielectric relaxation is through Cole-Cole model where the complex dielectric constant is known to be described by the emperical relation

$$\epsilon^\star = \epsilon' - i\epsilon'' = \epsilon_\infty + \frac{(\epsilon_s - \epsilon_\infty)}{1+(i\omega\tau)^{1-\alpha}}. \tag{3}$$

Here, ϵ_s and ϵ_∞ are low- and high-frequency values of ϵ', respectively, and α is a measure of the distribution of relaxation times. The experimental data are fitted to Eq. (3) and shown in Fig. 4, giving the values of α=0.102 and 0.12 at temperatures 263 and 303 K, respectively. A good agreement between the directly measured value of ϵ'' and those calcu-

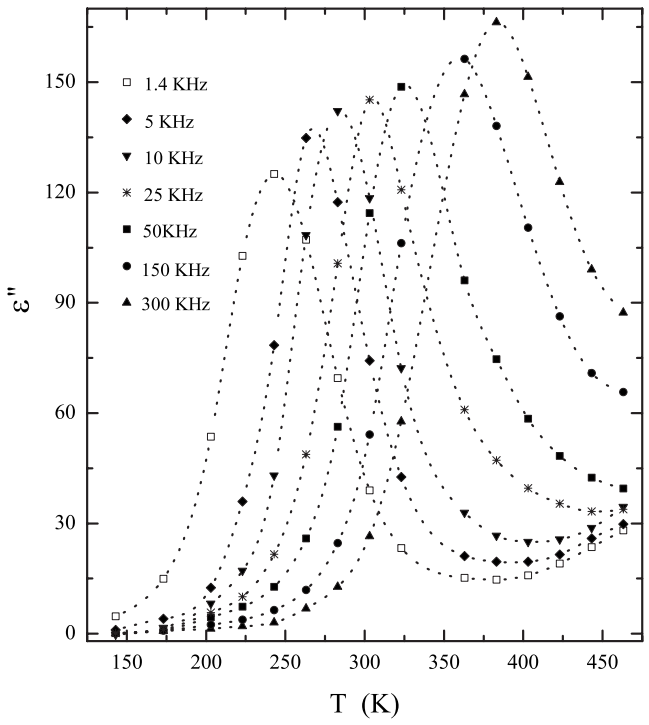

FIG. 3. Temperature dependence ϵ'' of $Ca(Fe_{1/2}Sb_{1/2})O_3$ at various frequencies.

lated using Eq. (3) suggests that the relaxation process differs from the monodispersive Debye process (for which $\alpha=0$). At

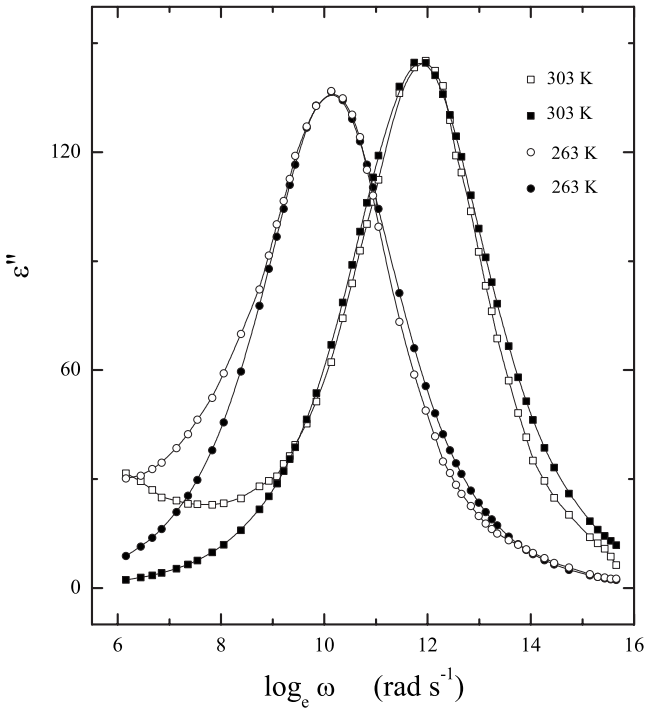

FIG. 4. Comparison of measured ϵ'' for $Ca(Fe_{1/2}Sb_{1/2})O_3$ with that calculated using Eq. (3) at temperatures 303 and 263 K. The open symbols represent the experimental points and solid symbols represent the calculated points.

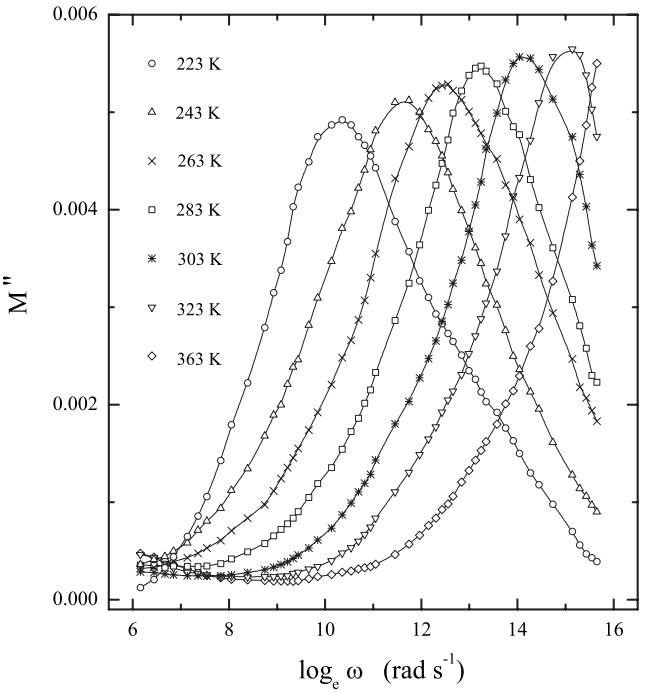

FIG. 5. Frequency dependence of M'' of $Ca(Fe_{1/2}Sb_{1/2})O_3$ at various temperatures.

303 K (Fig. 4) an increase in ϵ'' in the low-frequency region is due to dc conductivity.

We have also plotted the imaginary (M'') part of the complex electric modulus (M^*) as a function of frequency (angular) at several temperatures in Fig. 5. The frequency region below the peak maximum M''_{max} determines the range in which charge carriers are mobile on long distances. At frequencies above the peak maximum, the carriers are confined to potential wells, being mobile on short distances. The peak maximum M''_{max} increases with increasing temperature and shifts to the higher frequency side. At a temperature T, the most probable relaxation time corresponding to the peak position in tan δ vs $\log_e \omega$ and M'' vs $\log_e \omega$ is proportional to $\exp(-E_a/k_BT)$ (Arrhenius law) with activation energies $\simeq$0.60 and 0.61 eV, respectively, as shown in Fig. 6. Such a value of activation energy indicates that the conduction mechanism for CFS may be due to the polaron hopping based on the electron carriers. In the hopping process, the electron disorders its surroundings by moving its neighboring atoms from their equilibrium positions, causing structural defects in the B perovskite sites of the system. The preexponential factor obtained from the Arrhenius plot (Fig. 6) of tan δ is found to be $\simeq 2\times 10^{-10}$ s.

We have scaled each M'' by M''_{max} and each frequency by ω_{max}, where ω_{max} corresponds to the frequency of the peak position of M'' in the M'' vs $\log_e \omega$ plots in Fig. 7. The overlap of the curves at different temperatures into a single master curve indicates that the relaxation describes the same mechanism at various temperatures. We demonstrated a similar collapse of the $M''(\omega,T)$ data onto one single curve for $Sr(Fe_{1/2}Nb_{1/2})O_3$ (Ref. 6) and for $Ba(Al_{1/2}Nb_{1/2})O_3$ (Ref. 7).

Figure 8 shows the frequency dependence of the ac conductivity $\sigma(\omega)$ for CFS at different measuring temperatures.

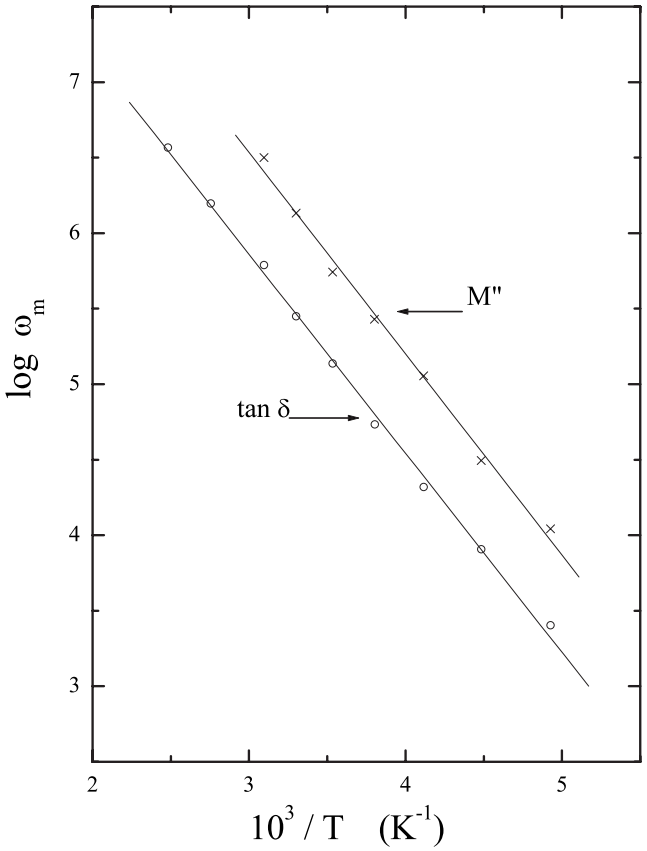

FIG. 6. The Arrhenius plot of ω_m corresponding to tan δ and corresponding to M''.

The real part of the ac conductivity can follow the power law,

$$\sigma' = \sigma_0 \left[1 + \left(\frac{\omega}{\omega_H} \right)^n \right], \tag{4}$$

where σ_0 is the dc conductivity, ω_H is the hopping frequency of the charge carriers, and n is the dimensionless frequency exponent. The conductivity shows a dispersion which shifts to higher frequencies with an increase in temperature. The experimental conductivity data were fitted to Eq. (4) with σ_0 and ω_H as variables, keeping in mind that the values of parameter n are weakly temperature dependent. Best fit data at 423 K (σ_0=0.0017, ω_H=8300 Hz, n=0.68) are shown in the inset of Fig. 8.

In Fig. 9, the variations of the normalized parameter M''/M''_{max} and tan δ/tan δ_{max} as a function of logarithmic frequency measured at 243 K for CFS are shown. For a delocalized or long range conduction, the peak position of two curves should overlap.[14] However, for the present system, the M''/M''_{max} and tan δ/tan δ_{max} peaks do not overlap, suggesting the components from both long range and localized relaxation. In order to mobilize the localized electron, the aid of lattice oscillation is required. In these circumstances, electrons are considered not to move by themselves but by hopping motion activated by lattice oscillation, i.e., the conduction mechanism is a considered as phonon-assisted hopping

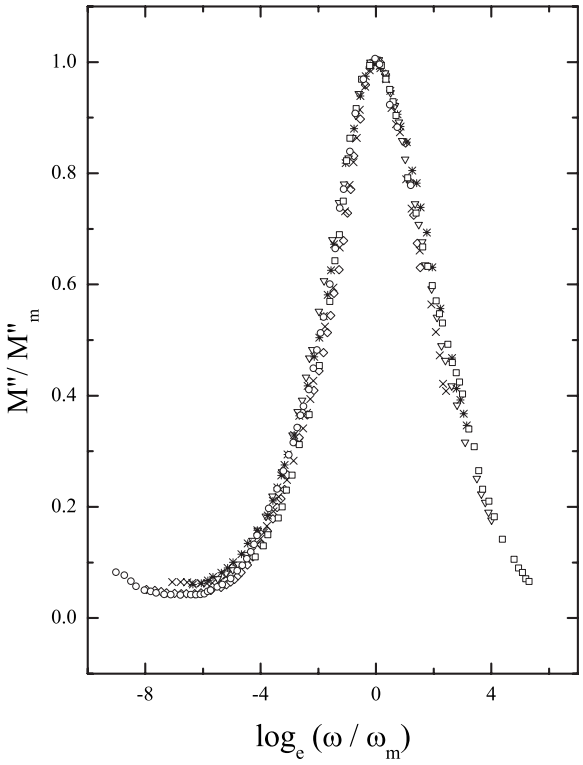

FIG. 7. Scaling behavior of M'' at various temperatures for $Ca(Fe_{1/2}Sb_{1/2})O_3$.

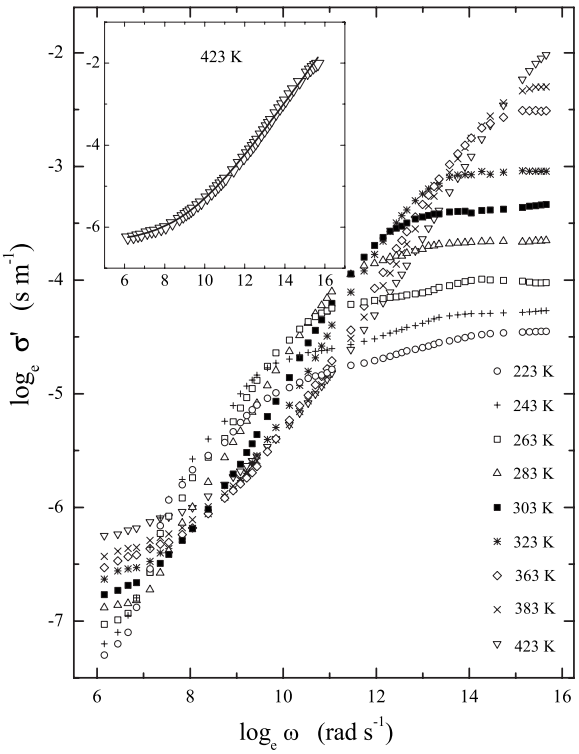

FIG. 8. Frequency spectra of the conductivity for $Ca(Fe_{1/2}Sb_{1/2})O_3$ at various temperatures. The solid line (inset) is the best fit to Eq. (4) at 423 K.

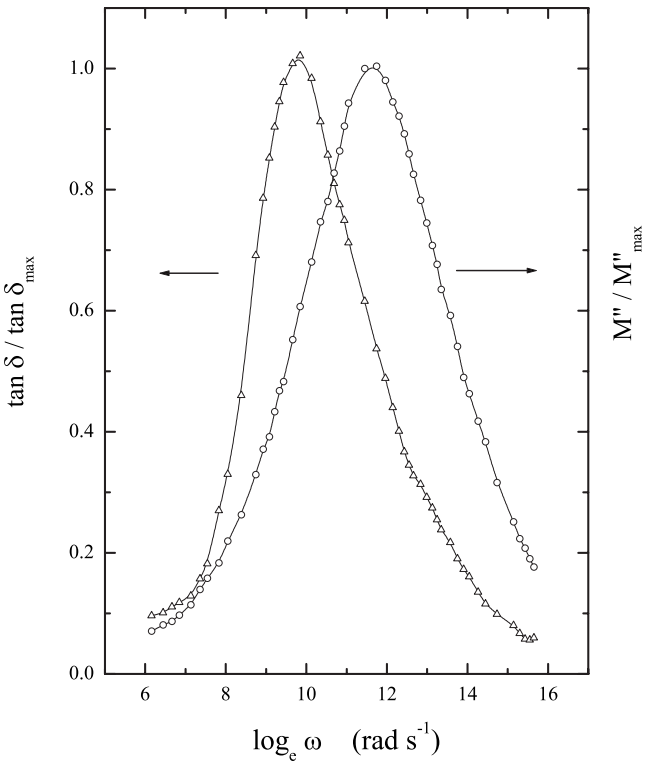

FIG. 9. Frequency dependence of normalized peaks, M''/M''_{max}, and tan δ/tan δ_{max} for $Ca(Fe_{1/2}Sb_{1/2})O_3$ at 243 K.

of small polaron between localized states. In addition, the magnitude of the activation energy suggests that the carrier transport is due to the hopping conduction.

Figure 10 shows the XPS spectrum of CFS in a wide energy range. The profiles of the XPS spectrum are identified and indexed in Fig. 10. The high resolution XPS spectra of the Fe $2p$ and Sb $3d$ states are shown in Figs. 11(a) and 11(b), respectively. The splitting of the Fe $2p$ state into $2p_{3/2}$ (713.1 eV) and $2p_{1/2}$ (726.6 eV) and of the Sb $3d$ state into $3d_{3/2}$ (542.26 eV) and $3d_{5/2}$ (532.7 eV) are due to the spin-orbit effect.[15] The spin-orbit splitting of the Fe $2p$ level is about 13.5 eV, while this is about 9.5 eV for Sb $3d$. The $2p$

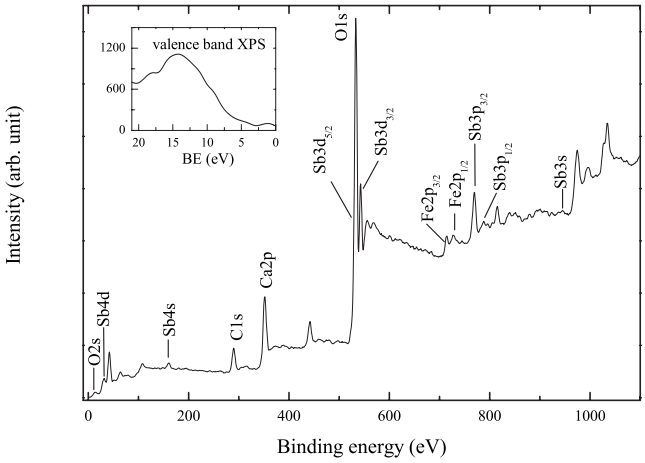

FIG. 10. XPS spectra of $Ca(Fe_{1/2}Sb_{1/2})O_3$.

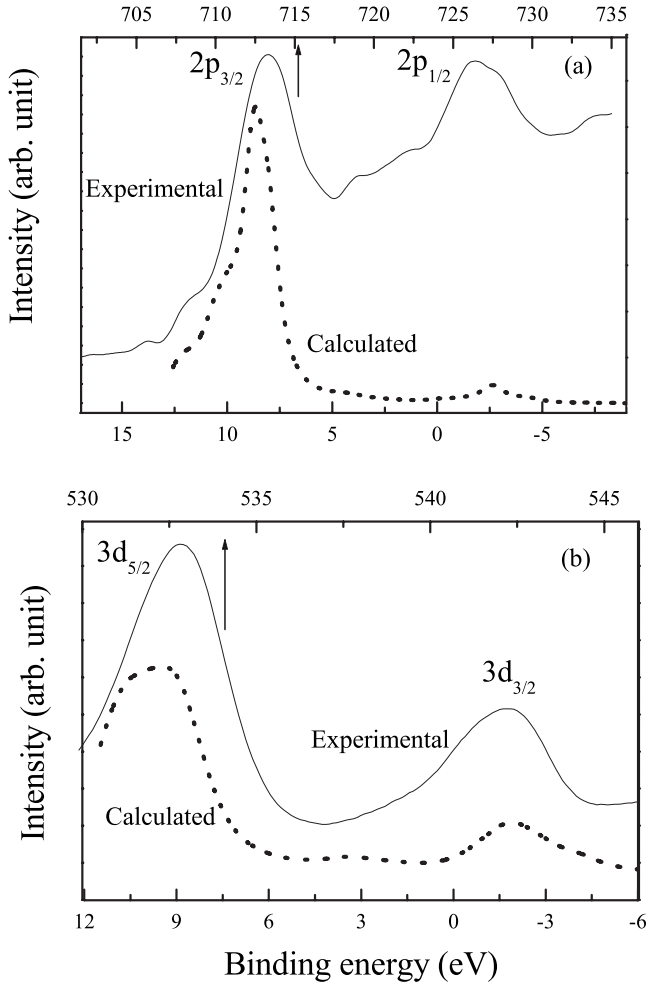

FIG. 11. The XPS and convoluted DOS spectra of the (a) Fe $2p$ state and (b) Sb $3d$ state for $Ca(Fe_{1/2}Sb_{1/2})O_3$.

region of compounds having an electronic configuration of d^5 has been extensively studied both theoretically[16] and experimentally.[17,18] Gupta and Sen[16] have calculated the multiplet structure of core p-vacancy levels in the Hartree-Fock free-ion approximation. They predict a large number of final states for a $2p$ vacancy, which will broaden the two main $2p$ lines asymmetrically and raise the background between $2p_{3/2}$ and $2p_{1/2}$. Qualitatively, this is the behavior observed in Fig. 11(a) for the Fe $2p$ spectrum. The presence of a distinct satellite around 718.8 eV in the Fe $2p_{3/2}$ peak indicates the dynamic charge transfer during the photoemission process, which appears in most of the XPS spectra of transition metal compounds.

The XPS investigation allows us to determine the relative concentrations of the constituents. The effective suppression of Fe^{2+} ions in CFS is confirmed by the XPS spectrum, which suggests a low concentration of oxygen vacancies, as shown in Fig. 11(a). As expected, the peak appearing at 713.1 eV and a satellite at 718.8 eV indicate the existence of Fe^{3+}, while the absence of peaks at 709.5 and 716 eV indicates an absence of Fe^{2+}.[19] The absence of Fe^{2+} and the low concentration of oxygen vacancies suggest an insulating resistivity for CFS, which should suppress many side effects

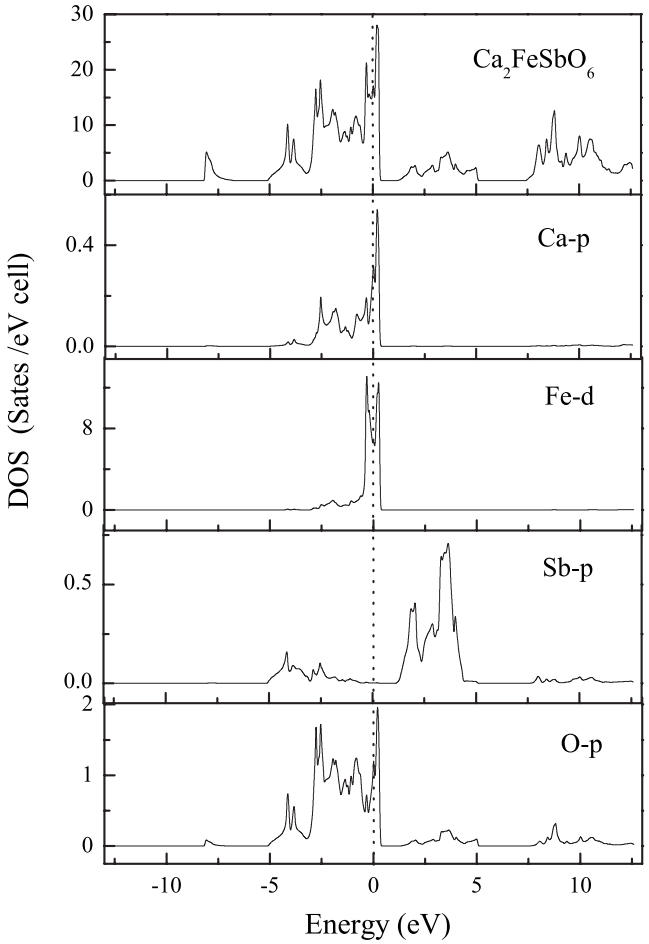

FIG. 12. Density of states of $Ca(Fe_{1/2}Sb_{1/2})O_3$ and partial density of states of Ca p, Fe d, Sb p, and O p.

arising from low resistivity, such as dielectric breaking under low electric field and/or unreal spontaneous electric polarization.[20] The inset of Fig. 10 shows the XPS spectrum of CFS presented on the binding energy (BE) scale from 0 to 21 eV (in the valence band region). The valence band photoemission spectra of CFS show a broad band centered at 14.3 eV with a shoulder at 11.7 eV and a less intense peak at 18 eV. These peaks have an Fe $3d$ electron character strongly hybridized to O $2p$ electrons. A less intense peak at about 1.15 eV comes from the nonbonding O p states with minimal contribution from Fe d states. These assignments will further be discussed.

The electronic structure and DOS of CFS are obtained by using the first-principles FLAPW method based on the GGA[21] within the frame work of DFT.[22] As mentioned earlier, the crystal structure of CFS is described by a monoclinic phase (a=5.9565 Å, b=6.9847 Å, and c=5.8047 Å) having volume 241 $Å^3$, we have computed the electronic structure and DOS of CFS in an undistorted $Fm3m$ double perovskite structure at the experimental volume ($a=2\times3.92$ Å).[2] A similar approach has been used by Cockayne to calculate the electronic structure and density of states of $CaAl_{1/2}Nb_{1/2}O_3$.[23]

Figure 12 shows the angular momentum decomposed total DOS with partial DOS of Ca p, Fe d, Sb p, and O p states. It is observed that the main contribution in valence band spectra comes from the O p state, and near the Fermi level (set at 0 eV) contribution comes from the Fe d state. The basic critical ingredients in the DOS are the d states of the Fe atom, which in term is split into t_{2g} and e_g states by the crystal field produced by the oxygen octahedra, with the t_{2g} states lower in energy and the e_g states higher in energy. The t_{2g} and e_g states are eigenstates to the Hamiltonian and do not hybridize with each other. In the scalar relativistic DOS, the threefold degenerate Fe t_{2g} states are filled. Therefore, the Fermi level ends up in the crystal-field gap between the Fe t_{2g} and e_g states.

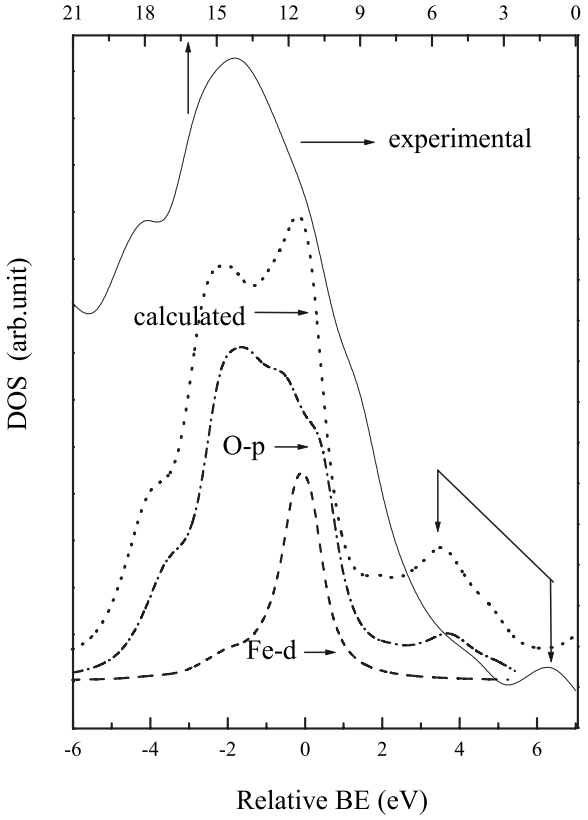

FIG. 13. The XPS spectrum in the valence band region is compared with the calculated spectra (by the FLAPW method).

The total DOS is convoluted with a Lorentzian of 0.5 eV full width at half maximum, and the calculated spectra are compared with the experimental XPS valence band spectra, as shown in Fig. 13. The calculated electronic structure of CFS is qualitatively similar to that of the XPS spectra in terms of spectral features, energy positions, and relative intensities. To get more insight into the valence band spectra near the Fermi level, we have also shown the convoluted angular momentum and site decomposed partial DOS of Fe d and O p in Fig. 13. It is clear from the calculated total DOS and partial DOS of O p and Fe d states that the broad peak at 14.3 eV arises from a bonding Fe(d)–O(p) interaction, whereas the less intense peak at 18 eV come from the O p states with negligible contribution from Fe d states. The shoulder appearing at 11.7 eV is contributed by the Fe d states, which are hybridized with the O p states. It further

confirms that the less intense peak at about 1.15 eV is due to the nonbonding state of O p. It seems that our DOS exhibits sharper peaks than the experimental spectra since we have not included the lifetime broadening in our DOS curve. The experimental bandwidth is larger than the calculated one. This reduction of bandwidth is due to the muffin-tin approximation, as we have observed in pure perovskites.[24,25] We have also compared the core level XPS spectra of Fe $2p$ and Sb $3d$ with the convoluted DOS data for Fe $2p$ and Sb $3d$, as shown in Figs. 11(a) and 11(b), respectively. Both the calculated spectra (dotted lines) appear to be very similar with the peak positions of XPS spectra, thus implying a good agreement between the experimental results and our theoretical calculations. From the above analysis we may conclude that the molecular formula for the ground state of CFS is $Ca_2^{2+}Fe^{3+}Sb^{5+}O_6^{2-}$.

IV. CONCLUSIONS

The frequency-dependent dielectric relaxation and conductivity of the CFS, $Ca(Fe_{1/2}Sb_{1/2})O_3$, ceramic synthesized by a solid-state reaction technique is investigated in the temperature range from 143 to 463 K. The x-ray diffraction of the sample at room temperature shows a monoclinic phase. The frequency dependence of the loss peak is found to obey an Arrhenius law with an activation energy of 0.60 eV. This value of activation energy suggests that the bulk conduction in CFS may be due to polaron hopping based on the electron carriers. Using the Cole-Cole model, an analysis of the imaginary part of the dielectric permittivity with frequency is performed, assuming a distribution of relaxation times. The presence of peak in the temperature dependence of the imaginary part of the dielectric constant $[\epsilon''(T)]$ indicates that the hopping of charge carriers is responsible for the dielectric relaxation. The scaling behavior of the imaginary part of the electric modulus (M'') suggests that the relaxation describes the same mechanism at various temperatures. The frequency-dependent conductivity spectra follow the power law. We studied the electronic structure of the CFS compound using XPS. The XPS spectrum was analyzed by first-principles full-potential linearized augmented plane wave method based on DFT under GGA. The calculated electronic structure of CFS is qualitatively similar to that of the XPS spectra in terms of spectral features, energy positions, and relative intensities.

ACKNOWLEDGMENTS

The authors thank Eric Cockayne of the Ceramic Division, Materials Science and Engineering Laboratory, National Institute of Standards and Technology, Gaithersburg, Maryland for sending his data on $CaTiO_3$ and $CaAl_{1/2}Nb_{1/2}O_3$ obtained by first-principles calculations and David J. Singh of the Oak Ridge National Laboratory, Oak Ridge for a helpful discussion on double perovskite. The authors are very much thankful to the referees for various suggestions to improve the quality of the manuscript.

[1] D. Viehland, S. J. Jang, L. E. Cross, and M. Wuttig, Phys. Rev. B **46**, 8003 (1992).
[2] S. Priya, A. Ando, and Y. Sakebe, J. Appl. Phys. **94**, 1171 (2003).
[3] I. Levin, J. Y. Chan, J. E. Maslar, and T. A. Vanderah, J. Appl. Phys. **90**, 904 (2001).
[4] R. Zurmuhlen, J. Petzett, S. Kamba, V. V. Voitsekhovskii, E. Colla, and N. Setter, J. Appl. Phys. **77**, 5341 (1995).
[5] S. Saha and T. P. Sinha, J. Phys.: Condens. Matter **14**, 249 (2002).
[6] S. Saha and T. P. Sinha, J. Appl. Phys. **99**, 014109 (2006).
[7] Alo Dutta and T. P. Sinha, J. Phys. Chem. Solids **67**, 1484 (2006).
[8] E. Iguchi, N. Kubota, T. Nakamori, N. Yamamoto, and K. J. Lee, Phys. Rev. B **43**, 8646 (1991).
[9] P. Blaha, K. Schwarz, G. Madsen, D. Kvasnicka, and J. Luitz, *WIEN2k: An Augmented Plane Wave+Local Orbitals Program for Calculating Crystal Properties* (Karlheinz Schwarz, Technische Universität Wien, Austria, 2001).
[10] E. Courtens, Phys. Rev. B **33**, 2975 (1986).
[11] E. Courtens, Phys. Rev. Lett. **52**, 69 (1984).
[12] S. L. Ginzburg, *Irreversible Phenomena of Spin Glasses* (Nauka, Moscow, 1989).
[13] L. Lindgren, P. Svedlindh, and O. J. Beckman, J. Magn. Magn. Mater. **25**, 33 (1981).
[14] R. Gerhardt, J. Phys. Chem. Solids **55**, 1491 (1994).
[15] M. Abbate, H. Ascolani, F. Prado, and A. Caneiro, Solid State Commun. **129**, 113 (2004).
[16] R. P. Gupta and S. K. Sen, Phys. Rev. B **10**, 71 (1974).
[17] S. P. Kowalczyk, L. Ley, F. R. McFeely, and D. A. Shirley, Phys. Rev. B **11**, 1721 (1975).
[18] J. A. Tossell, J. Electron Spectrosc. Relat. Phenom. **10**, 169 (1977).
[19] W. Eerenstein, F. D. Morrison, J. Dho, M. G. Blamire, J. F. Scott, and N. D. Mathur, Science **307**, 1203a (2005).
[20] X. D. Qi, J. Dho, R. Tomov, M. G. Blamire, and J. L. MacManus-Driscoll, Appl. Phys. Lett. **86**, 062903 (2005).
[21] J. P. Perdew, J. A. Chevary, S. H. Vosko, K. A. Jackson, M. R. Pederson, D. J. Singh, and C. Fiolhais, Phys. Rev. B **46**, 6671 (1992).
[22] P. Hohenberg and W. Kohn, Phys. Rev. **136**, B864 (1964).
[23] Eric Cockayne, J. Appl. Phys. **90**, 1459 (2001).
[24] S. Saha, T. P. Sinha, and A. Mookerjee, Phys. Rev. B **62**, 8828 (2000).
[25] S. Saha, T. P. Sinha, and A. Mookerjee, J. Phys.: Condens. Matter **12**, 3325 (2000).